# NMR Studies of the Phosphorylation Motif of the HIV-1 Protein Vpu Bound to the F-Box Protein $\beta$-TrCP†

Gaël Coadou,‡ Josyane Gharbi-Benarous,‡ Simon Megy,‡ Gildas Bertho,‡ Nathalie Evrard-Todeschi,‡ Emmanuel Segeral,§ Richard Benarous,§ and Jean-Pierre Girault*,‡

*Laboratoire de Chimie et Biochimie Pharmacologiques et Toxicologiques, UMR 8601 CNRS, Université René Descartes, Paris V, 45 rue des Saint-Pères, 75270 Paris Cedex 06, France, and Département des Maladies Infectieuses, Institut Cochin, U567 INSERM, UMR 8104 CNRS, Hôpital Cochin Bat. G. Roussy, 27 rue du Faubourg St. Jacques, 75014 Paris, France*

*Received July 9, 2003; Revised Manuscript Received September 18, 2003*

ABSTRACT: A protein−protein association regulated by phosphorylation of serine is examined by NMR studies. Degradation of the HIV receptor CD4 by the proteasome, mediated by the HIV-1 protein Vpu, is crucial for the release of fully infectious virions. Phosphorylation of Vpu at two sites, Ser52 and Ser56, on the motif DSGXXS is required for the interaction of Vpu with the ubiquitin ligase SCF-$\beta$TrCP which triggers CD4 degradation by the proteasome. This motif is conserved in several signaling proteins known to be degraded by the proteasome. To elucidate the basis of $\beta$-TrCP recognition, the bound conformation of the P-Vpu$^{41-62}$ peptide was determined by using NMR and MD. The TRNOE intensities provided distance constraints which were used in simulated annealing. The $\beta$-TrCP-bound structure of P-Vpu was found to be similar to the structure of the free peptide in solution and to the structure recognized by its antibody. Residues 50−57 formed a bend while the phosphate groups are pointing away. The binding fragment was studied by STD-NMR spectroscopy. The phosphorylated motif D**pS**$^{52}$GNE**pS**$^{56}$ was found to make intimate contact with $\beta$-TrCP, and pSer52 displays the strongest binding effect. It is suggested that Ser phosphorylation allows protein−protein association by electrostatic stabilization: an obvious negative binding region of Vpu was recognizable by positive residues (Arg and Lys) of the WD domain of $\beta$-TrCP. The Ile46 residue was also found essential for interaction with the $\beta$-TrCP protein. Leu45 and Ile46 side chains lie in close proximity to a hydrophobic pocket of the WD domain.

Vpu[1] is an 81-residue membrane-associated accessory protein encoded in the HIV-1 genome (Figure 1a). Vpu is specific for HIV-1, the major causative agent of the acquired immune deficiency syndrome (AIDS) and is not found in HIV-2 (which is less pathogenic than HIV-1) or in most simian immunodeficiency viruses (SIV) (*1*, *2*). It was shown (Figure 1b) that its secondary structure consists of one transmembrane hydrophobic helix (h1) near the N-terminus and two amphipathic helices (h2 in-plane and h3) in the cytoplasmic C-terminal domain, using a combination of solid-state NMR and solution NMR methods (*3*). The protein has two biological activities that contribute to the virulence of HIV-1 infections in humans (Figure 2a). It enhances the release of new virus particles from cells infected with HIV-1 and induces the intracellular degradation of the CD4 receptor protein (*4*, *5*) by targeting it for proteolysis by the ubiquitin−proteasome pathway (*6*). Both activities contribute to increased virion production (*7*). These functions appear to be associated with two different structural domains of Vpu (*8*, *9*). The N-terminal transmembrane helix, which serves as a membrane anchor, is required to regulate virus secretion, most likely by formation of an ion channel. The cytoplasmic domain of Vpu, which has two phosphorylation sites (pSer52 and pSer56), is essential for interaction with CD4 and induction of CD4 degradation in the endoplasmic reticulum (ER). The mechanism by which Vpu mediates CD4 degradation has been elucidated (Figure 2a). It has been demonstrated that, by binding to the F-box WD40 protein $\beta$-TrCP, the receptor component of the SCF E3 ubiquitin ligase $\beta$-TrCP, Vpu can subvert the cellular targeting pathways to the proteasome in order to promote CD4 degradation (*6*). Phosphorylation of Ser52 and Ser56 of Vpu by casein kinase 2 (*10*, *11*) is necessary for interaction with $\beta$-TrCP (*12*, *13*). Vpu-induced degradation of CD4 requires, in fact, the formation of multiprotein complexes containing CD4, Vpu, $\beta$-TrCP, Skp1, and other subunits of the SCF E3 ubiquitin ligase (*6*) and the function of the proteasome (*14*, *15*).

† This work was supported by grants from organizations involved in AIDS and cancer research: ANRS (Agence Nationale pour la Recherche contre le SIDA), SIDACTION, ARC, and Ligue Nationale contre le Cancer. E.S. is supported by the ARC.

* To whom correspondence should be addressed. Tel: 01 42 86 21 80. Fax: 01 42 86 83 87. E-mail: girault j@biomedicale.univ-paris5.fr.

‡ LCBPT, CNRS, Université René Descartes, Paris V.

§ U567 INSERM, UMR 8104 CNRS, Institut Cochin, Département des Maladies Infectieuses, Hôpital Cochin Paris.

[1] Abbreviations: $\beta$TrCP, transducin repeat containing protein; GST, glutathione *S*-transferase; HIV, human immunodeficiency virus; HSQC, heteronuclear single-quantum correlation; INEPT, insensitive nuclei enhanced by polarization transfer; MD, molecular dynamics; NOESY, nuclear Overhauser effect spectroscopy; PBS, phosphate-buffered saline; rmsd, root mean square deviation; SCF, Skp1-Cullin-FBox; STD, saturation transfer difference; TRNOESY, transferred nuclear Overhauser effect spectroscopy; TOCSY, total correlation spectroscopy; TPPI, time-proportional phase incrementation; Vpu, HIV-1 encoded virus protein U; WATERGATE, water suppression by gradient-tailored excitation; WD domain, Trp Asp domain.

10.1021/bi035207u CCC: $25.00 
Published on Web 11/21/2003

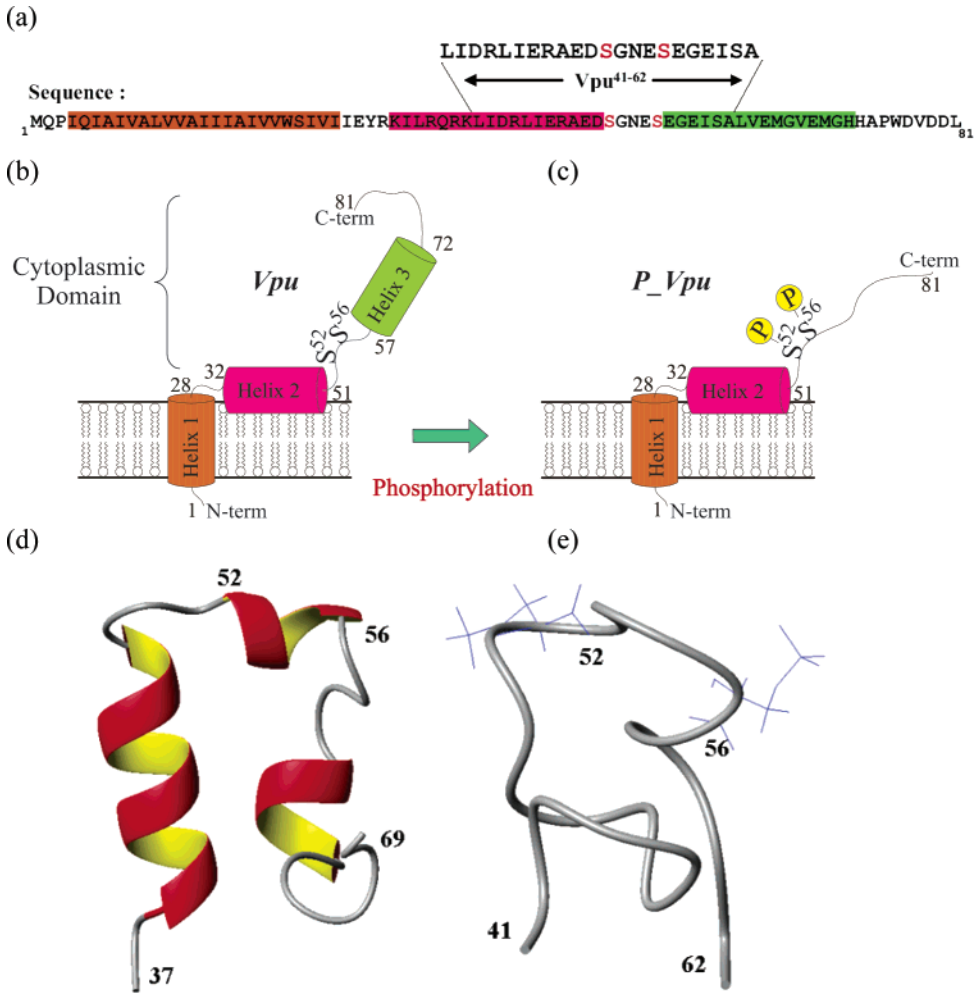


FIGURE 1: (a) Primary structure sequence of the HIV-1 Vpu protein and, above, the sequence of the Vpu fragment which was investigated in the present work. (b) Domains of the secondary structural regions found in Vpu. The hydrophobic N-terminal membrane anchor (1−28) is followed by two amphipathic α-helices (helix h2, 32−51; helix h3, 57−72). Both helices are joined by a flexible nonstructured link, which contains the phosphoacceptors Ser52 and Ser56. The C-terminus forms a reverse turn at $Ala^{74}$ (*39*). (c) Domains of the secondary structural regions found in P-Vpu which contains the phosphoserines pSer52 and pSer56 and in which helix 3 disappears. (d) Part of the backbone (37−69) of the Vpu cytoplasmic domain (37−81) structure (*18*). (e) Backbone (41−62) of the minimum energy-minimized conformer of the free P-$Vpu^{41-62}$ peptide at pH 7.2.

Human β-TrCP, which specifically associates with Vpu, is a member of the WD protein family (Figure 2b) (*6*). This WD repeat protein (Figure 3) of particular interest appears to have no individual repeat specializations and to have minimum-length strand-connecting loops and turns (*16*). These may provide fixed platforms onto which one can attach de novo designed peptides with predicted catalytic functions. Human β-TrCP is composed of two main domains. An F-box near the N-terminus is involved in interaction with Skp1, a connecting factor to the other subunits of the SCF E3 ligase complex for ubiquitin-mediated proteolysis. At the C-terminus, the seven WD repeats (Figure 3) are necessary and sufficient for binding protein substrates of β-TrCP which are phosphorylated on the DSGXXS phosphorylation motif. The ternary complexes of CD4, Vpu, and β-TrCP provide direct evidence for the function of Vpu as an adapter molecule that links CD4 to β-TrCP (Figure 2a). Evidence has been provided that Vpu−β-TrCP interaction depends on the phosphorylation of Vpu on the motif DSGXXS, which is found in several cellular signaling proteins known to be subjected to degradation by the proteasome. This motif is found in cellular signaling proteins such as IκBα, the inhibitor of the master transcription factor NFκB, and β-catenin, the accumulation of which has been implicated in various human cancers. Indeed, it has been shown that IκBα and β-catenin are cellular substrates of β-TrCP (*13*). Hence, all substrates of β-TrCP, either viral like Vpu or cellular like IκBα or β-catenin, share a similar motif of the type DSGXXS. The phosphorylation of the motif on the two serine residues is required for interaction with β-TrCP and the subsequent targeting of these substrates to be degraded by the proteasome. Thus, the elucidation of the mechanism involved in Vpu recognition by β-TrCP upon phosphorylation of this DSGXXS motif is essential if one wants to understand how HIV-1 can subvert this ubiquitin−proteasome cellular pathway controlled by β-TrCP (Figure 2a) to degrade CD4 and to produce fully infectious particles.

In our previous study, the structural influence of phosphorylation at the two sites, Ser52 and Ser56, of the P-$Vpu^{41-62}$ peptide (numbers refer to the Vpu protein) and its effect on the relatively flexible interconnection between the two α-helices, h2 and h3, have been examined. The intrinsic conformational properties of the free P-$Vpu^{41-62}$ peptide LIDRLIERAED**pS**GNE**pS**EGEISA (numbers refer

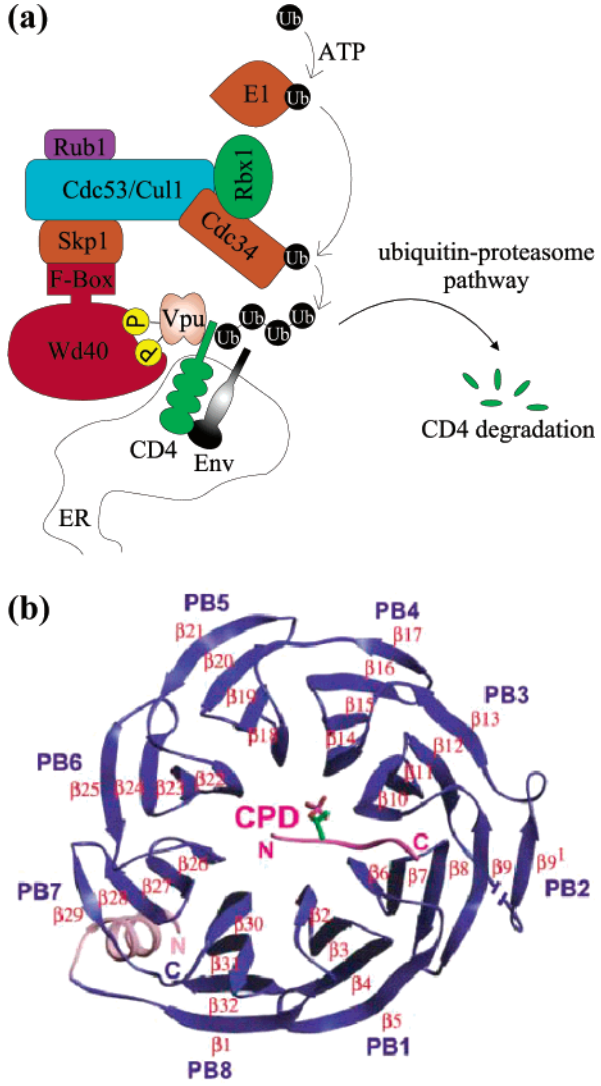


FIGURE 2: (a) A schematic of how a $\beta$-TrCP-binding peptide that is derived from the HIV Vpu protein is phosphorylated by active casein kinase for ubiquitination and degradation by the proteasome. Several F-box proteins can recognize short phosphopeptide motifs that correspond to substrate sequences. The F-box protein $\beta$-TrCP binds the doubly phosphorylated consensus motif D**pS**GXX**pS** in I$\kappa$B$\alpha$, $\beta$-catenin, and Vpu in an analogous manner to Cdc4. (b) Ribbons diagram of the eight $\beta$-propeller structure of the WD40 repeat region of the yeast F-box protein Cdc4 which is homologous to $\beta$-TrCP. Peptide recognition as seen in the X-ray crystal structure of the complex (Cdc4−CPD peptide) (*44*).

to the Vpu protein) were investigated in phosphate-buffered solution, using NMR and molecular modeling simulation (*17*). Simulations, in accordance with NMR experiments, showed that the P-Vpu$^{41-62}$ phosphorylated peptide analogue (Figure 1e) has different structural features than the parent Vpu$^{41-62}$ peptide (Figure 1d) (*18*). The relative disorder of the h3 helix (57−69) can be accounted for by the structural rearrangements triggered by phosphorylation.

We now report the conformation of the D**pS**GXX**pS**-containing peptide P-Vpu$^{41-62}$ bound to the protein $\beta$-TrCP by TRNOE NMR spectroscopy (*19, 20*). To provide additional information for the peptide mode of binding, the saturation transfer difference (STD-NMR) technique, a method of epitope mapping by NMR spectroscopy, has been performed (*21*−*23*). Determining the $\beta$-TrCP-bound P-Vpu$^{41-62}$ peptide conformation is an essential step toward understanding how the Vpu molecular activities affect the biological functions essential for the viral life cycle. Thus, determination of the conformational features of the P-Vpu (D**pS**GXX**pS**) moiety implicated in the protein $\beta$-TrCP binding should provide information in a more general context, i.e., on the structural parameters characterizing Vpu−$\beta$-TrCP receptor interaction. This should contribute to the design of molecules mimicking the structure of the Vpu adhesion site and possibly thus acting as a potent model for the D**pS**GXX**pS**−$\beta$-TrCP complex. Because $\beta$-TrCP is responsible for several important biological functions, the Vpu D**pS**GXX**pS**−$\beta$-TrCP complex is an attractive candidate for structure determination.

## MATERIALS AND METHODS

*Reagents*. HIV-1 encoded virus protein U (Vpu) fragments (41−62), Vpu$^{41-62}$ with the amino acid sequence LIDRLIERAEDSGNESEGEISA, and the peptide P-Vpu$^{41-62}$ containing the phosphorylated sites 52 and 56, Ser($PO_3H_2$), LIDRLIERAED**pS**GNE**pS**EGEISA, were purchased from Neosystem Laboratory, Strasbourg, France. The purity (95%) of the peptides was tested by analytical HPLC and by mass spectrometry.

*Purification of the WD Repeat Region from Human Protein $\beta$-TrCP Fused to GST*. The coding sequence corresponding to residues 251−569 of the full-length protein $\beta$-TrCP was inserted into the pGEX-4T2 expression vector (Amersham) as previously described (*6*). The construction resulted in a fusion protein of approximately 60 kDa corresponding to the 218 residues of the GST, a 18-mer linker, and the seven WD repeats (residues 251−569) of $\beta$-TrCP (Figure 3), hereafter named GST-$\beta$-TrCP.

Saturated overnight cultures (10 mL) of *Escherichia coli* BL21 transformed with pGEX-4T-2::TrCP WD were diluted 1:100 with 1 L of Luria−Bertani medium (LB) containing ampicillin (50 mg/L) and allowed to grow until they reached $OD_{600}$ = 0.6 at 37 °C. Then the culture was placed at 4 °C for 30 min, and the fusion protein expression was induced with 0.5 mM isopropyl $\beta$-D-thiogalactopyranoside (IPTG) and ethanol (2% v/v) for 3 h at 30 °C. After centrifugation at 4000 rpm for 30 min at 4 °C, the solution was dissolved in 100 mL of lysis phosphate buffer (PBS) containing 2 mM EDTA, 0.5% Triton, 1 mM dithiothreitol (DTT), and 1 mL of a protease inhibitor cocktail (Sigma). Then lysozyme (0.5 mg/mL) was added to the buffer, and the suspension was placed at 4 °C for 1 h with gentle shaking. The solution was finally disrupted by sonication, and cell debris was removed by centrifugation for 45 min at 4 °C at 10000 rpm. Glutathione−Sepharose 4B beads (Pharmacia-Biotech) were centrifuged at 7000 rpm for 2 min and washed twice with PBS. A total of 2.5 mL of beads was added to the crude lysates, and the binding of GST to glutathione was allowed for 2 h at 4 °C, with gentle shaking. The beads were then washed three times with NaCl (1 M) to remove the nonspecific binding and three times with PBS. GST-$\beta$-TrCP from *E. coli* BL21 was eluted by competition with reduced glutathione. Beads, loaded with GST-$\beta$-TrCP, were equilibrated in PBS, and the fusion protein was eluted by the addition of 5 mL of ice-cold PBS (pH 8) containing 10 mM reduced glutathione. The supernatant was separated from the beads by centrifugation, and a second elution was performed

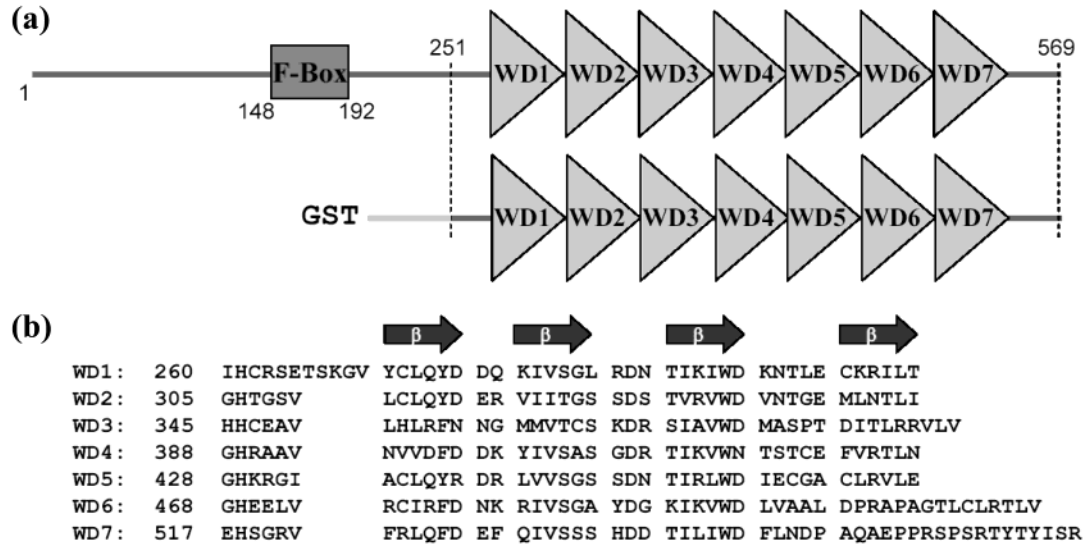


FIGURE 3: (a) The full-length human protein $\beta$-TrCP and, below, the fusion GST-$\beta$-TrCP protein which was investigated in the present work. This recombinant protein includes the 218 residues of the glutathione *S*-transferase (GST) protein fused to the seven WD repeats (residues 251−569) of the full-length protein $\beta$-TrCP by an 18 residue linker. (b) The WD repeats were identified in the primary sequence of $\beta$-TrCP from their alignment with the regular expression.

following the same protocol. The solutions were analyzed by SDS−PAGE (12%) (Figure S9a in the Supporting Information). A Western blot analysis was also performed to check the recognition of the protein using anti-$\beta$-TrCP polyclonal antibodies (C-18) from Santa Cruz (Figure S9b).

Protein concentration was determined using the standard Bradford and Coomassie Brilliant Blue method, following the OD at 595 nm. Finally, the purified recombinant protein was concentrated using Amicon Ultra-15 centrifugal filter units from Millipore with a 30 kDa molecular mass cutoff. The solution was washed in NMR buffer and concentrated several times, performing a buffer exchange in order to remove the excess reduced glutathione. Following this protocol, the final yield of purified GST-$\beta$-TrCP from 1 L of Luria−Bertani medium (LB) was about 1.2 mg. This amount of purified recombinant protein was used to prepare the NMR samples.

*NMR Spectroscopy*. $^1$H NMR and STD spectra were recorded with a Bruker AMX-500 spectrometer. Standard Bruker software was used to acquire and process the NMR data. NMR samples contained the P-Vpu$^{41-62}$ peptide with the GST-$\beta$-TrCP protein. They were prepared in phosphate-buffered saline solution, pH 7.2 (20 mM phosphate, 5% $D_2O$, 0.02% $NaN_3$).$^1$H NMR spectra were recorded at constant temperature (280 K) and at pH 7.2. The NMR samples were adjusted to a protein concentration of 0.2 mM on the basis of the visible absorption at 595 nm. A 10-fold ligand excess (2 mM) over binding sites was used throughout the studies. One sample control was prepared containing the nonphosphorylated peptide, Vpu$^{41-62}$ with the GST-$\beta$-TrCP protein (Figure S10b in the Supporting Information). Resonances of the peptide were assigned on the basis of 2D TOCSY and NOESY experiments. Water suppression was achieved by WATERGATE (*24*). Chemical shifts were referenced to internal TSP-$d_4$ [3-(trimethylsilyl)propionic acid-*2,2,3,3*-$d_4$ sodium salt] (Tables 1 and 2). 2D TRNOESY spectra were recorded to determine the most favorable ratio for transferred NOE effects, which was found to be 10:1. TRNOESY experiments were performed with mixing times of 100, 200, and 400 ms for molar ratios between 50:1 and 5:1. After optimization of the P-Vpu$^{41-62}$ peptide:protein ratio, the final sample was prepared with 5 mg of GST-$\beta$-TrCP protein (0.2 mM protein) and 2.5 mg of P-Vpu$^{41-62}$ peptide (2 mM; 10:1 peptide:binding site ratio) in 500 $\mu$L of buffer (Figure S10a in the Supporting Information). TRNOESY experiments were acquired in the phase-sensitive mode using the States−TPPI method, with 4K points and 512 $t_1$ increments and a relaxation delay of 1.5 s, and the mixing time of the maximum transfer NOE determined from buildup curves was 200 ms.

Table 1: $^1$H NMR Chemical Shifts of the Free Peptide P-Vpu$^{41-62}$ in ppm from TSP-$d_4$[a]

| residue | $\delta$NH | $\delta H_\alpha$ | $\delta H_\beta$ | $\delta H_\gamma$ | $\delta H_\delta$ | $\delta$ others |
|---|---|---|---|---|---|---|
| Leu41 | − | 4.06 | 1.73, 1.67 | 1.67 | 0.97 | |
| Ile42 | − | 4.22 | 1.85 | 1.52, 1.22 | 0.89 | |
| Asp43 | 8.60 | 4.59 | 2.74, 2.59 | | | |
| Arg44 | 8.43 | 4.32 | 1.88, 1.78 | 1.64 | 3.22 | 7.37, 7.02, 6.65 |
| Leu45 | 8.53 | 4.34 | 1.73, 1.63 | 1.61 | 0.96, 0.89 | |
| Ile46 | 8.05 | 4.17 | 1.88 | 1.50, 1.21 | 0.91, 0.88 | |
| Glu47 | 8.58 | 4.28 | 2.04, 1.94 | 2.28, 2.24 | | |
| Arg48 | 8.45 | 4.38 | 1.89, 1.79 | 1.66 | 3.22 | 7.45, 7.02, 6.65 |
| Ala49 | 8.71 | 4.32 | 1.45 | | | |
| Glu50 | 8.60 | 4.28 | 2.10, 1.96 | 2.31 | | |
| Asp51 | 8.39 | 4.67 | 2.78, 2.70 | | | |
| pSer52 | 8.91 | 4.52 | 4.12 | | | |
| Gly53 | 8.74 | 4.00 | | | | |
| Asn54 | 8.38 | 4.80 | 2.87, 2.76 | 7.87, 7.05 | | |
| Glu55 | 8.73 | 4.34 | 2.11, 1.98 | 2.32 | | |
| pSer56 | 8.87 | 4.55 | 4.11, 4.06 | | | |
| Glu57 | 8.78 | 4.30 | 2.13, 2.00 | 2.34 | | |
| Gly58 | 8.44 | 4.03, 3.93 | | | | |
| Glu59 | 8.41 | 4.32 | 2.03, 1.95 | 2.30, 2.24 | | |
| Ile60 | 8.48 | 4.23 | 1.89 | 1.53, 1.23 | 0.94 | |
| Ser61 | 8.61 | 4.49 | 3.87 | | | |
| Ala62 | 8.22 | 4.16 | 1.37 | | | |

[a] Spectra were recorded at 280 K, pH = 7.2, and 20 mM sodium phosphate buffer; $H_2O$:$^2H_2O$, 9:1 (by volume). Resonances of protons marked by a dash were not visible.

Table 2: $^1$H NMR Chemical Shifts of the Peptide P-Vpu$^{41-62}$ Bound to the Protein $\beta$-TrCP in ppm from TSP-$d_4$[a]

| residue | $\delta$NH | $\delta H_\alpha$ | $\delta H_\beta$ | $\delta H_\gamma$ | $\delta H_\delta$ | $\delta$ others |
|---|---|---|---|---|---|---|
| Leu41 | − | 4.04 | 1.73 | 1.65 | 0.96 | |
| Ile42 | − | 4.20 | 1.84 | 1.50, 1.20 | 0.98 | |
| Asp43 | 8.61 | 4.59 | 2.72, 2.58 | | | |
| Arg44 | 8.45 | 4.29 | 1.92, 1.81 | 1.62 | 3.21 | 7.35 |
| Leu45 | 8.51 | 4.32 | 1.70 | 1.58 | 0.94 | |
| Ile46 | 8.10 | 4.14 | 1.86 | 1.47, 1.19 | 0.90 | |
| Glu47 | 8.57 | 4.27 | 1.93, 2.08 | 2.24 | | |
| Arg48 | 8.49 | 4.34 | 1.85, 1.76 | 1.64 | 3.21 | 7.44 |
| Ala49 | 8.69 | 4.31 | 1.42 | | | |
| Glu50 | 8.59 | 4.25 | 1.94, 2.09 | 2.29 | | |
| Asp51 | 8.40 | 4.65 | 2.77, 2.69 | | | |
| pSer52 | 9.03 | 4.47 | 4.10 | | | |
| Gly53 | 8.73 | 3.98 | | | | |
| Asn54 | 8.37 | 4.79 | 2.85, 2.75 | 7.88, 7.06 | | |
| Glu55 | 8.70 | 4.33 | 1.97, 2.11 | 2.30 | | |
| pSer56 | 8.91 | 4.52 | 4.07, 4.02 | | | |
| Glu57 | 8.80 | 4.28 | 2.00, 2.13 | 2.30 | | |
| Gly58 | 8.46 | 4.00 | 3.92 | | | |
| Glu59 | 8.42 | 4.31 | 1.92, 2.01 | 2.23, 2.29 | | |
| Ile60 | 8.49 | 4.22 | 1.86 | 1.51, 1.26 | | |
| Ser61 | 8.62 | 4.49 | 3.85 | | | |
| Ala62 | 8.23 | 4.14 | 1.35 | | | |

[a] Spectra were recorded at 280 K, pH = 7.2, P-Vpu/$\beta$-TrCP = 10, and 20 mM sodium phosphate buffer; $H_2O$:$^2H_2O$, 9:1 (by volume). Resonances of protons marked by a dash were not visible.

For STD experiments (Figure 4) the ligand-to-protein ratio was raised to 50:1 (0.2 mM P-Vpu$^{41-62}$ peptide, 40 $\mu$M GST-$\beta$-TrCP protein). The time dependence of the saturation transfer was investigated by recording STD spectra with 1024 scans and saturation times from 0.2 to 4.0 s. STD-NMR spectra for the P-Vpu$^{41-62}$ peptide mode of binding were acquired using a series of equally spaced 50 ms Gaussian-shaped pulses for selective saturation, with 1 ms delay between the pulses, and a total saturation time of approximately 2 s (Figure 4a). With an attenuation of 50 dB, the radio frequency field strength for the selective saturation pulses in all STD-NMR experiments was 190 Hz. The frequency of the protein (on-resonance) saturation was set to the protein $^1$H NMR signals in the low-frequency region −3 ppm. It was observed that setting the saturation at the aromatic region of the on-resonance frequency saturated amido, guanidino, and carboxamido protons of the ligand. The off-resonance saturation frequency was set at 30.0 ppm. Subtraction of FID values with on- and off-resonance protein saturation was achieved by phase cycling. As no baseline distortion was observed, no $T_{1\rho}$ filter was applied to eliminate the background resonances of the GST-$\beta$-TrCP protein. A total relaxation delay of 1.7 s and eight dummy scans were employed to reduce subtraction artifacts. 1K total scans (or 10K for a better signal-to-noise ratio) were collected. Relative STD values were calculated by dividing STD signal intensities by the intensities of the corresponding signals in a 1D $^1$H NMR reference spectrum of the same sample recorded with 256 scans. 2D STD inverse correlation ($^1$H−$^{13}$C) phase-sensitive HSQC experiments (Figure 4c) were recorded using echo/anti-echo gradient selection with decoupling during acquisition (*25*). The 2D $^1$H/$^{13}$C correlation was obtained via double INEPT transfer using a TRIM pulse of 0.2 ms duration. One millisecond half-sinusoid echo/anti-echo gradients of 40, 10 G/cm with recovery delay of 200 $\mu$s, were used. To select protons attached to carbon, a delay of 1.78 ms was optimum for C−H one-bond couplings: delay = $1/(4^1J_{C-H})$. This technique is optimized to obtain $C_\alpha$−$H_\alpha$ correlations with a sensitivity enhancement. The spectra were recorded with 256 experiments of 2048 data points and 48 scans per $t_1$ experiment. Subtraction of the on- and off-resonance spectra was made by phase cycling, respectively. The acquisition times for the 2D experiments were typically around 10 h with a relaxation delay (Aq + $D_1$) of 1.7 s. All spectra were processed with Bruker Xwinnmr software. 2D spectra were multiplied with 90°-shifted squared sine bells in both dimensions and zero-filled two times. HSQC experiments have allowed us to assign the $^{13}$C resonances. Assignments in $H_2O$ obtained at 280 K were reported in Tables S4 and S5 in the Supporting Information for the free and bound P-Vpu$^{41-62}$ peptide, respectively.

*Structure Calculation*. NMR spectra were analyzed with FELIX software (Biosym Technologies). The P-Vpu$^{41-62}$ chemical shifts were assigned using the standard technique (*26*). Distance restraints used in the structure calculations were derived from TRNOESY experiments performed with mixing times of 100 and 200 ms (Figure 5); as for the free ligand, we obtained a blank TRNOESY spectrum at 100 ms and only sequential NH/$H_\alpha$ correlations at 200 ms. They were based on TRNOE peak intensities and were classified as strong, medium, or weak restraints, corresponding to distance restraints of 1.8−2.7, 1.8−3.6, and 1.8−6.0 Å, respectively. The distance between the two Asn $NH_2$ protons (1.78 Å) was used as a reference for calibration. The final list of distant restraints containing 183 unambiguous and 38 ambiguous restraints was incorporated for structure calculation with the standard protocol of ARIA 1.2 (*27*−*29*). The simulated annealing protocol consisted of four stages: a high-temperature torsion angle simulated annealing phase at 10000 K (1100 steps), a first torsion angle dynamics cooling phase from 10000 to 2000 K (550 steps), a second Cartesian dynamics cooling phase from 2000 to 1000 K (5000 steps), and a third Cartesian dynamics cooling phase from 1000 to 0 K (2000 steps). ARIA runs were performed using the default parameters with eight iterations. Twenty structures were generated each round, and the 10 lowest energy structures were carried to the next iteration. The peptide structures were determined and further refined using molecular dynamics with the parallhdg 5.3 force field. Modifications to the force field for the phosphorylated residues (pSer) were made with CHARMM (*30*) and reported for MD simulations. A total of 18 $\phi$ dihedral angles were constrained between −20° and −180° (usually the only range considered in NMR-derived structures) (*31*), the region of a Ramachandran plot populated by nearly all non-glycyl residues. While ARIA allows the final structures to undergo a procedure in a simulated water box, it was decided that due to the presence of the bound peptide in the hydrophobic recognition sites this step was not applicable. After the final iteration, with ARIA software (OPLS force field), 20 structures were generated and retained as the final structures. The final list of distant restraints contained 221 restraints divided into 41 intraresidue NOEs and 96 sequential, 63 medium-range, and 21 long-range contacts. Analysis of the ARIA results (Table 3) was carried out using the aria.overview script (*32*). The final PDB structures were analyzed and visualized with AQUA, PROCHECK-NMR (*33*), and MOLMOL (*34*) programs.

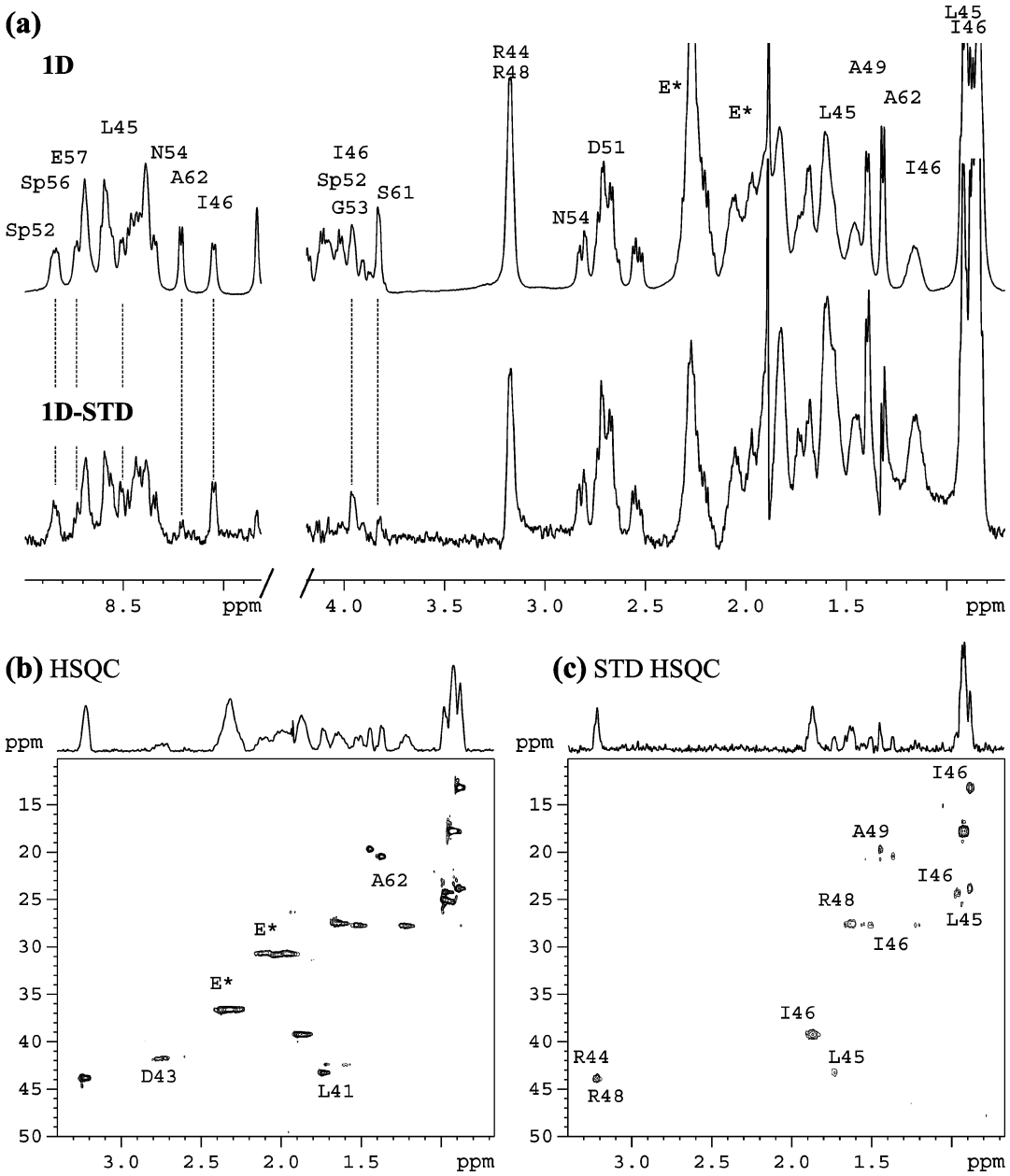


FIGURE 4: (a) 1D $^1$H spectrum (top) and 1D $^1$H STD-NMR spectrum (bottom) of the P-Vpu$^{41-62}$ peptide in association with the GST-$\beta$-TrCP protein, showing enhancements of resonances of protons making close contacts with the protein combining site. (b) Reference 2D HSQC region spectrum of the complex P-Vpu$^{41-62}$−GST-$\beta$-TrCP protein. (c) The corresponding 2D STD-HSQC region spectrum. The Glu47, Glu50, and Glu55 residues are identified with the one-letter amino acid code and an asterisk, because of resonance overlapping.

## RESULTS

*NMR Experiments for the Peptide−β-TrCP Protein Complex*. Addition of 0.2 mM GST-$\beta$-TrCP caused a line broadening of the P-Vpu$^{41-62}$ signals and a chemical shift difference relative to the free peptide (Figure 6), thus providing a clear indication of the existence of binding. NOESY and TOCSY spectra allowed for the complete assignment of the peptide (Table 2). The bound conformation of the peptide was investigated by TRNOESY experiments (Figure S10a in the Supporting Information). The P-Vpu$^{41-62}$ peptide, which is a large molecule with a relatively long correlation time, gives already negative NOEs in the free state. By comparison of buildup rates of the P-Vpu$^{41-62}$ peptide NOEs with and without GST-$\beta$-TrCP, the cross-peaks proved to be, in fact, real TRNOEs. The maximum of the buildup curve moved from about 500 ms without protein to 200 ms in the presence of GST-$\beta$-TrCP. A NOESY NMR experiment of the nonphosphorylated Vpu$^{41-62}$ peptide in the presence of the GST-$\beta$-TrCP protein was performed as a reference experiment, at the same concentration as that used for the P-Vpu$^{41-62}$−GST-$\beta$-TrCP sample. The addition of the Vpu$^{41-62}$ peptide (2 mM) to the GST-$\beta$-TrCP protein (0.2 mM) results in the absence of any broadening of all the peaks in the control spectrum. A negative control was obtained thanks to a blank TRNOESY spectrum with mixing times of 100 ms, and the NOESY spectrum of the free Vpu$^{41-62}$ with only sequential NH/H$_\alpha$ correlations, when the mixing time was 200 ms (Figure S10b in the Supporting Information). This showed that the large number of negative NOEs observed with P-Vpu$^{41-62}$ in the presence of the fusion GST-$\beta$-TrCP protein was due to transfer from the bound peptide (transferred NOEs). Moreover, the $\beta$-TrCP-bound P-Vpu$^{41-62}$


FIGURE 5: Sequential and medium-range TRNOE connectivities in the peptides P-Vpu$^{41-62}$ (sequence at the top) in the presence of the GST-$\beta$-TrCP protein at 5 °C and pH 7.2. The thickness of the lines reflects the relative intensities of the NOEs within the individual plots. $d_{NN}$, $d_{\alpha N}$, and $d_{\beta N}$ represent sequential NOE connectivities; $d_{\alpha N}(i,i+2)$ and $d_{\alpha N}(i,i+3)$ are medium-range NOE connectivities between α- and $\beta$-protons or α- and amide protons.

Table 3: Structural Statistics of the Final 10 NMR Structures of P-Vpu$^{41-62}$ Bound to $\beta$-TrCP Protein

| ARIA$_{output}$ | |
|---|---|
| no. of exptl distance restraints | |
| unambiguous NOE | 183 |
| ambiguous NOE | 38 |
| total NOEs | 221 |
| no. of exptl broad dihedral restraints | 18 |
| rms differences from distance restraints[a] | |
| unambiguous NOE (Å) | 0.15 ± 0.07 |
| ambiguous NOE (Å) | 0.07 ± 0.07 |
| all NOEs (Å) | 0.13 ± 0.06 |
| NOE violations >0.5 Å | 5 |
| NOE violations >0.3 Å | 7 |
| rms differences from mean structure[b] (Å) | |
| backbone | 2.02 ± 0.96 |
| heavy | 3.27 ± 1.14 |
| Ramachandran plot of residues[c] | |
| in most favored regions | 45 |
| in additional allowed regions | 28 |
| in generously allowed regions | 27 |
| in disallowed regions | 0 |

[a] Calculated by ARIA. [b] Calculated by MOLMOL. [c] Calculated by PROCHECK.

structure was found to be very similar to the structure recognized by anti-phosphorylated Vpu antibody. A novel phosphorylation-specific monoclonal antibody (mAb DE7-24) was generated against the P-Vpu$^{41-62}$ peptide. The mAb-bound P-Vpu$^{41-62}$ peptide conformation is finally being elucidated and is going to be published. Thus, determination of the structural properties of the P-Vpu$^{41-62}$ peptide, when bound to a monoclonal antibody directed against P-Vpu$^{41-62}$, should provide information on the structural parameters characterizing P-Vpu−$\beta$-TrCP receptor interaction. Several transferred NOE contacts were observed in the presence of the GST-$\beta$-TrCP protein (Figure 5). Only the amide proton of Ile42 was invisible, which led to an ill-defined N-terminal part of the ligand.

The structures generated using ARIA resulted in TRNOE restraint files consisting of 183 unambiguous and 38 ambiguous distance restraints (Table 3). Among these TRNOEs, those that were possibly ambiguous were given the most logical assignment as determined by the sequence. To determine between the probable contribution for each of the ambiguous NOEs, the automated assignment program ARIA

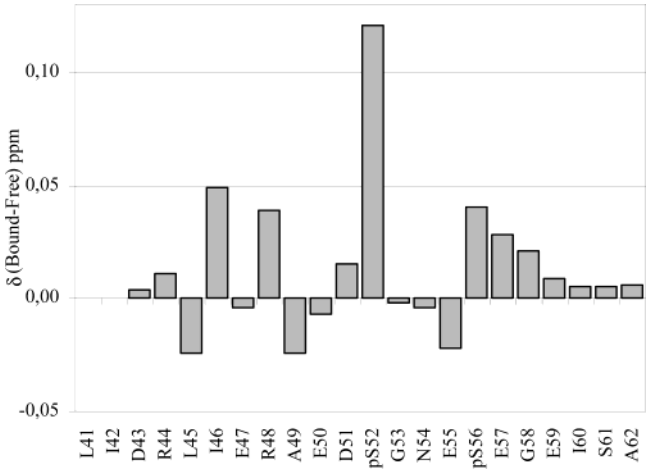


FIGURE 6: Difference for the 22 residues of P-Vpu$^{41-62}$ between the chemical shift of a given resonance free in buffer solution and the chemical shift in the presence of the GST-$\beta$-TrCP protein plotted against residue number at 5 °C and pH 7.2 for NH resonances.

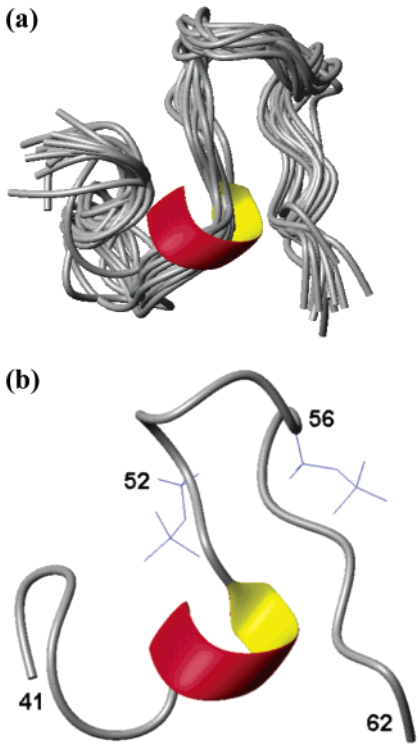


FIGURE 7: NMR TRNOE-derived structures of the bound peptide P-Vpu$^{41-62}$ in the presence of the GST-$\beta$-TrCP protein. (a) Twenty structures were generated after eight iterations with ARIA software. (b) The minimum energy-minimized conformer with the best fit of proton distance constraints.

was used. Various runs were performed with ARIA to utilize as many unambiguous and ambiguous restraints as possible from the 500 MHz TRNOESY spectra, and the lowest energy structures were retained. The final statistics of these structures are presented in Table 3. The bound P-Vpu$^{41-62}$ peptide showed a structured helical N-terminal part, residues 43−49, and a large bent ED**pS**$^{52}$GNE**pS**$^{56}$E, from residue Glu50 to residue Glu57 (Figure 7). The 20 structures superimposed with rmsd = 2.02 Å for backbone atoms, or 3.27 Å for all heavy atoms, considering the entire peptide (Table 3).

The interaction causes environmental changes on the peptide−protein interfaces and, hence, affects the chemical

shifts of the nuclei in this area. Shifts perturbations are very sensitive to subtle effects. The perturbations of the chemical shifts are recorded in Figure 6. We follow the NH resonances to their bound position, and we extract the binding constant by fitting the fractional shift against an equation depending on total $\beta$-TrCP protein and P-Vpu$^{41-62}$ ligand concentrations (*19*, *35*). Fast exchange was measured for the interaction of the phosphorylated P-Vpu$^{41-62}$ peptide to the $\beta$-TrCP protein with a dissociation constant of around 100 $\mu$M. The amide proton of the phosphorylated pSer52 shifted ≈0.12 ppm downfield, whereas the Ile46, Arg48, and pSer56 amide protons were shifted slightly downfield (≈0.05 ppm) and to a lesser extent were (≈0.03 ppm) the NH's of Asp51, Asn54, Glu55, Glu57, and Gly58. This suggests a possible interaction of the negative phosphorylated side chain of the pSer52 amino acid with positively charged residues in the $\beta$-TrCP protein. For pSer56 an ionic interaction with the charged group may play a partial role at a longer distance from the phosphorylation site. No shifting resonances were observed with the control sample of the nonphosphorylated Vpu$^{41-62}$ peptide in the presence of GST-$\beta$-TrCP.

*STD-NMR Experiments of P-Vpu$^{41-62}$ in the Presence of the $\beta$-TrCP Protein*. To describe the region responsible for the binding interaction of the P-Vpu$^{41-62}$ peptide with GST-$\beta$-TrCP, specific affinity was investigated by STD-NMR spectroscopy experiments (*21*, *22*) to study the influence of the serine phosphorylation on binding (Figure 4). Optimization of the experimental setup for STD-NMR spectroscopy was achieved using samples without any GST-$\beta$-TrCP protein present. In that case, STD spectra did not contain ligand signals, because saturation transfer does not occur without the protein. Only the sample containing the GST-$\beta$-TrCP protein showed saturation transfer from the protein to the ligand in the STD spectra. Investigation of the time dependence of the saturation transfer with saturation times from 0.2 to 4.0 s showed that 2 s was sufficient for efficient transfer of saturation from the protein to the ligand protons. The signals of the NH and aliphatic groups present in STD spectra showed similar behavior (Figure 4). The analysis of the relative STD intensities of P-Vpu$^{41-62}$ was accomplished by integrating the dispersed proton resonances and referencing them to one of the most intensive proton signals, the NH of the pSer52 (or Ile46) residue. The 1D NMR spectra shown in Figure 4a reveal that a direct analysis of the integrals of individual proton resonances in the aliphatic region is impeded due to severe signal overlap by the intense resonances of the corresponding methyl groups. Nevertheless, the spectral region corresponding to the amino protons is well resolved and can be used to classify the amino acid residues relevant for interaction with the $\beta$-TrCP. Additionally, the $H_\beta$ and methyl resonances of the residues are indicated in the STD spectrum and show large STD intensities. Comparison of the STD spectrum with the corresponding 1D $^1$H NMR spectrum (Figure 4a) clearly demonstrated the involvement of the NH (44−57), the aliphatic protons ($H_\beta$ or $H_\gamma$) of Arg44, Leu45, Ile46, Arg48, Ala49, Asp51, and Asn54, and the methyl group of Leu45 and Ile46 in binding. As shown in Figure 4a, it is clear that NH (8.2 ppm) of the C-terminal residue (Ala62) is not observed in the difference spectrum; STD spectra did not contain the characteristic $H_\beta$ signal of Ala62.

The 1D $^1$H NMR spectrum of P-Vpu$^{41-62}$ in the presence of the GST-$\beta$-TrCP protein showed signals belonging to glutathione used during a first GST-$\beta$-TrCP protein purification to elute the protein (Figure S11 in the Supporting Information). They were not present in the corresponding STD spectra because this impurity does not bind to the $\beta$-TrCP protein. Recording STD-NMR experiments of the nonphosphorylated Vpu$^{41-62}$ peptide in the presence of GST-$\beta$-TrCP protein also provided a negative control. This control experiment was one experimental way to distinguish between specific effects of binding peptide to its target and nonspecific interactions between the ligand and macromolecular complex. In that case, STD spectra did not contain ligand signals; no effects are observed as enhancements of the signals of protons that could be in close contact with the protein (Figure S12 in the Supporting Information). Thus, saturation transfer does not occur without the D**pS**$^{52}$GNE**pS**$^{56}$ motif. This showed that the large number of the enhancements observed for the P-Vpu$^{41-62}$ peptide in the presence of the GST-$\beta$-TrCP protein was due to the areas of the ligand actually contacting the $\beta$-TrCP binding site.

The same sample was also used for a 2D STD-HSQC experiment. Figure 4b shows a region of the HSQC spectrum and Figure 4c the corresponding region of the STD-HSQC spectrum. Again, one can observe how signals corresponding to residues in close proximity to the receptor are saturated to a higher degree, resulting in more intense cross-peaks. The traces corresponding to the $H_\beta/C_\beta$ Leu45 and Ile46, as well as the $H_\beta/C_\beta$ Arg48, Ala49, and Asp51, are present from the spectrum in Figure 4c, providing that they have interaction with the $\beta$-TrCP protein. As evident from integrals of the 2D STD-HSQC spectrum, proton resonances of Ile46 and pSer52 have the highest intensities, signals of Arg48, Ala49, and Asp51 are of medium intensity, while the signals of Ser61 have the lowest intensity. No cross-peaks issued from $H_\beta/C_\beta$ Ile60 or Ala62 residues can be seen due to their low degree of saturation. In agreement with the 1D STD experiment, the strongest signals are again those corresponding to residues 44−48 of the cytoplasmic domain and the loop region (residues 51−56) involving pSer52. The peaks of pSer56 are low in intensity; this residue has a weaker contact to the protein surface than the phosphorylated residue pSer52 of the P-Vpu$^{41-62}$ ligand. When the signals in the 1D spectra are not well enough resolved, the binding epitope could be determined from 2D cross-peak integrals. It was clear from these data that the P-Vpu$^{41-62}$ peptide bound weakly to $\beta$-TrCP, as indicated by positive response in TRNOESY spectra (Figure S10 in the Supporting Information) and selective binding in the $^1$H STD-NMR spectra (Figure 4).

## DISCUSSION

*Vpu-Mediated CD4 Degradation*. Vpu-induced degradation of CD4 requires in fact the formation of multiprotein complexes containing CD4, Vpu, and $\beta$-TrCP (Figure 2) (*6*). The published data show that the cytoplasmic domain of HIV-1 Vpu binds directly to part of the cytoplasmic domain (402−420) of the CD4 receptor (*8*). Residues important for direct interaction with CD4 were mapped by a mutational study (*36*) using a yeast two-hybrid system. Deletion of amino acids in the Glu47−Ser56 region results in loss of CD4 degradation activity (*37*). Mutation of the Leu41 residue

does not affect CD4 binding activity, but Ile46 does. Deletion of residues 41−48 also abolishes CD4 binding activity (*36*).

*Ternary Complexes of Vpu, CD4, and β-TrCP*. The ability of Vpu to independently interact with CD4 or β-TrCP requires that both proteins can simultaneously interact with Vpu. The presence of ternary complexes clearly demonstrates that Vpu acts as a linker molecule between CD4 and β-TrCP (Figure 2a), and it indicates that the binding sites of Vpu to CD4,are distinct. The two conserved phosphoserine residues (Ser52/Ser56) located in the cytoplasmic domain of Vpu are known to be essential for the ability of Vpu to induce CD4 degradation, but they are not required for Vpu interaction with CD4. On the contrary, these former residues are required for binding of Vpu to β-TrCP, since the double mutant Vpu S52N/S56N has lost its ability to interact with β-TrCP (*6*).

*Vpu Protein*. The structural studies of the nonphosphorylated Vpu protein by the Synchrotron X-ray reflectivity technique (*38*) indicated (Figure 1b) that the hydrophobic transmembrane helix (h1) is oriented approximately normal to the plane of the monolayers while the amphipathic α-helices of the cytoplasmic domain lie on the surface of the phospholipid headgroups (*3*). The solution structure of the Vpu cytoplasmic domain (Figure 1d), the nonphosphorylated peptide $Vpu^{32-81}$, consists of a helix (h2), a loop region, a helix (h3), and a C-terminal turn (*18*, *39*). Ser52 and Ser56, located in the hinge region between the two helices (h2 and h3) (Figure 1b), are phosphorylated by casein kinase II (CKII) (Figure 1c). Then they are required for binding of Vpu to β-TrCP to promote CD4 degradation (*13*). The structure of the free P-$Vpu^{41-62}$ phosphorylated peptide by NMR spectroscopy and restrained molecular dynamics shows that the peptide adopts in solution (Figure 1e) a helical N-terminal part, a bend including the phosphorylation motif D**pS**$^{52}$GNE**pS**$^{56}$, and a flexible extended "tail" for the C-terminal part (*17*).

*The Bound Conformation of P-$Vpu^{41-62}$ to the Protein β-TrCP*. The bound conformation of the P-$Vpu^{41-62}$ peptide (Figure 7) was investigated by TRNOESY experiments. A large number of transferred NOE contacts were observed in the presence of the GST-β-TrCP protein (Figure 5). For the segment 41−49, the short distances, $d_{\alpha N}(i,i+3)$, between Leu41 and Arg44, Arg44 and Glu47, and Leu45 and Arg48 provided an indication for the presence of a short helix. This turn region is characterized by Ramachandran angles in the α-helical region (Table S6 in the Supporting Information). The bound conformation of segment 41−49 falls partly into the same regular α-helix h2 of the free phosphorylated peptide, P-$Vpu^{41-62}$. A large bend involves the P-$Vpu^{41-62}$ peptide segment of eight residues, 50−57. This bend or hairpin loop is characterized by two Ramachandran angle regions where the $\psi$ torsion angles (residues 50−52 and residues 54−56) have opposite signs. In this bend, strong sequential NOEs and NOE-observable short distances $d_{\alpha N}(i,i+2)$ between Asp51 and Gly53 and between Asn54 and pSer56 constrain $\psi$ to torsion angles resulting in a half-turn structure. The P-$Vpu^{41-62}$ peptide in the bound state exhibits chemical shift variation involving residues of this loop region. The loop contains those residues that show the lowest rmsd value (0.23 Å for residues 51−56) of their backbone coordinates. The flexible tail (residues 58−62) is in an extended form because only strong sequential NOE $d_{\alpha N}$'s are observed. NOEs corresponding to long-range backbone distances (Glu50, Ile60) then showed that segments 49−51 and 58−60 form a rather β-strand. The overall negative potential generated by the seven aspartic and glutamic acid residues increases with the phosphorylated Ser52 and Ser56. Thus, in the bound P-$Vpu^{41-62}$ peptide, the negative electrostatic potential dominates the peptide surface completely.

*The Binding Region of P-$Vpu^{41-62}$ with β-TrCP*. STD-NMR spectroscopy (*21*) offers an efficient alternative approach to identify the residues involved in binding to receptor proteins. A prerequisite for STD-NMR spectroscopy is that the ligand is reversibly bound to the protein. The binding affinity ($K_d$) should be in the range of 1 mM to 10 nM. The observed low binding affinity of P-$Vpu^{41-62}$ with β-TrCP, in the range of approximately 0.1 mM, allowed the performance of STD-NMR spectroscopy. By acquiring STD-HSQC spectra, the aliphatic chains of the components with binding activity were readily assigned (Figure 4c). The pSer52 residue gives intensive STD signals corresponding to a tight contact to the protein. Strong STD signals are observed also for Gly53, Asn54, and pSer56, which are weakly bound, resulting in smaller integrals. Comparison of the STD spectrum with the corresponding 1D $^1$H NMR spectrum (Figure 4a) demonstrated the involvement of the NH groups of the six-residue sequence D**pS**GXX**pS** in binding. Mean STD values (in percent) calculated for each amino acid from the 1D $^1$H STD-NMR and 2D STD-HSQC spectra showed a 2-fold more effective saturation transfer for the protons of the pSer52 residue compared to the motif showing a sufficient saturation transfer. The Glu50, Asp51, Ser($PO_3^{2-}$)52, Glu55, Ser($PO_3^{2-}$)56, and Glu57 residues form a negative surface that provides a plausible binding region.

As evident from Figure 4, signals of Leu45, Ile46, and Arg48 are also of high intensity, while the amide proton and the chain protons of Ile60, Ser61, and Ala62 were invisible. It could be shown that apart the diphosphorylated segment (51−56), other groups in close proximity (44−48) were also involved in binding. Obviously, pSer52 and Ile46 get more saturation from the protein than the remaining residues of the ligand and therefore have more and tighter contacts to the β-TrCP's surface. Similarities are observed between Vpu and other proteins known to be degraded by the proteasome pathway. IκBα, which binds to the transcription factor NFκB, is ubiquitinated and degraded through the proteasome pathway. Two amino acid sequences in IκBα are known (*15*) to play an important role in this process: a six amino acid diserine motif, D**pS**GLD**pS**, and about nine amino acids upstream of the phosphoserine motif, two lysine candidate sites in the binding sequence RLLD, for covalent attachment of ubiquitin. In the same relative position Vpu contains a closely related, repeated sequence, RLIE. Both the diserine motif D**pS**GNE**pS** (51−56) and the RLIER (44−48) motif in Vpu are in contact with the protein β-TrCP.

The distribution of the shifts of the backbone protons along the sequence was also indicative of a bound fraction due to shorter distances between protons of the ligand and protein. An ionic interaction with the charged end groups may play a partial role. In the presence of β-TrCP interaction, the NH resonance of pSer52 moves significantly and to a lesser extend the NH of Ile46 and the NH's of segment 54−57. For pSer52 the effect is slightly stronger than for pSer56 in the bound peptide. This may reflect a higher affinity for pSer52, where the phosphorylation leads to a direct effect

on the population of the preferred backbone structure with the necessity of ionic interaction.

Interaction of HIV-1 Vpu with $\beta$-TrCP relies on motif D**pS**GNE**pS**, similar to that found in the other substrates of $\beta$-TrCP (I$\kappa$B$\alpha$ and $\beta$-catenin). It is interesting to note that the first serine residue of this motif seems to play an essential role in this interaction. The second serine residue is involved in the case of Vpu and $\beta$-catenin but not required for the interaction of ATF4 with $\beta$-TrCP (ATF4, a member of the family of transcription factors). Interaction of ATF4 with $\beta$-TrCP relies on motif DSGXXXS (*40*). The phosphorylated side chain is Ser, Thr, or His. Often this residue is preceded or followed by a Gly; in most cases the residue two positions further along the chain is a positively charged Lys or Arg. These sequences bear some resemblance to the phosphoryl-binding loop of various proteins (*41*).

*$\beta$-TrCP Binding Site for P-Vpu*. Various proteins bind a phosphoryl moiety at a characteristic site. This may be a loop between a carbonyl end of a $\beta$-strand and a following $\alpha$-helix. This may be explained by a favorable electrostatic interaction between the negative charge of the phosphoryl group and the dipole of the $\alpha$-helix (*42*).

Two major domains can be distinguished in $\beta$-TrCP (Figure 3). The N-terminal domain contains an F-box motif (residues 148−192) (Figure 3a) identified as a sequence involved in the recruitment of $\beta$-TrCP to the SCF multisubunit E3 ubiquitin ligase complex through interaction with Skp1 (Figure 2a) (*43*). The C-terminal domain of $\beta$-TrCP contains seven WD repeats (Figure 3b), known to form interfaces for protein−protein interaction (*16*). The N-terminal domain of $\beta$-TrCP comprising the F-box motif did not interact with Vpu. The C-terminal fragment of $\beta$-TrCP with the seven WD repeats was sufficient for binding to Vpu. Deletion of the first WD domain abolished the interaction with Vpu (*6*). In contrast, a weak interaction was still detected with mutants lacking either the C-terminal tail after the seventh WD domain or WD repeats 4−7. Although the first WD motif seems to be particularly important for interaction with Vpu, all seven WD repeats as well as the C-terminal end are required for optimal binding. The $\beta$-TrCP protein is not the only example of a WD-like protein that recognizes a defined peptide sequence. The analysis of an X-ray crystal structure published recently reveals the binding site specific for a phosphopeptide complex bound to an eight-bladed WD40 propeller domain in the $SCF^{Cdc4}$ ubiquitin ligase (Figure 2b) (*44*). Other seven-blade propellers, such as "clathrin" containing WD repeats, recognize some of their interaction targets through peptide-in-groove interactions (*45*). A small number of amino acids, located and also tightly clustered on one side of the $\beta$-propeller, interact with their partners (*46*).

$\beta$-TrCP could associate with the P-$Vpu^{41-62}$ peptide via charge-based interactions. The WD domain of $\beta$-TrCP has positive amino acids that could accept the diphosphorylated segment D**pS**GXX**pS** present in the Vpu, $\beta$-catenin, and I$\kappa$B$\alpha$ protein. The Lys or Arg residues of the WD1 fragment would be part of the $\beta$-TrCP interaction domain with the acidic-rich P-Vpu segment, wherein 30% of the residues are aspartic or glutamic acids and phosphorylated groups. To test the specific association between the WD-repeat domain of the receptor subunit of the $SCF^{\beta-TrCP}$ ubiquitin ligase and a phosphorylated I$\kappa$B$\alpha$ peptide (pI$\kappa$B$\alpha$), the effect of the Lys mutant residues (WD1, Lys304 and Lys326 by alanine) on binding P-I$\kappa$B$\alpha$ was examined (*47*). A single WD1, Lys326 mutation has an inhibitory effect on the binding of P-I$\kappa$B$\alpha$. It was suggested that the phosphate groups form also direct electrostatic interactions with the guanidium groups of Arg in the WD domain and direct hydrogen bonds with the side chain of Tyr residues as in the X-ray crystal structure of the phosphopeptide−Cdc4 complex (*44*). On the basis of previous mutational analysis (*48*−*50*), these Arg residues are essential for function.

A second absolute requirement for the P-$Vpu^{41-62}$−$\beta$-TrCP complex rests on Ile46 and Leu45, the side chains of which may project into a three-sided pocket on the WD40 surface. $\beta$-TrCP displays, from the STD experiment (Figure 4a), a strong interaction with the hydrophobic residues Leu/Ile at the 45 and 46 positions of the P-$Vpu^{41-62}$. The Leu/Ile side chains fit into a hydrophobic pocket that would be composed of the hydrophobic residues Trp, Met, Leu, Thr, and Val of the WD surface.

Modeling of the F-box protein $\beta$-TrCP (*51*) reveals an extensive basic region on the front face of the propeller, which may engage substrate phosphoepitopes. The $\beta$-TrCP WD domain has the ability to recognize pSer epitopes in the context of the adjacent Gly residue while in the X-ray crystal structure of the phosphopeptide−Cdc4 complex, the Cdc4 WD domain employs a pThr-Pro peptide (*44*, *48*). The Pro or the Gly binding pocket is able to accommodate other residues with a same propensity to form $\beta$ turns. The specificity of phosphorylation recognition by the WD domain of $\beta$-TrCP and Cdc4 is characterized by a dedicated pSer-Gly or pThr-Pro binding pocket, an hydrophobic pocket that selects hydrophobic residues N-terminal to the phosphorylation site.

This work has allowed us to determine which sequence requirements in addition to the D**pS**GXX**pS** motif are playing a role in interaction with $\beta$-TrCP. The bent region (51−56) of the bound P-$Vpu^{41-62}$ peptide associated with the hydrophobic cluster (45−46) characterizes the phosphorylation-dependent recognition by the WD domain.

## CONCLUSION

The backbone resonance assignments of the bound P-$Vpu^{41-62}$ peptide led to the determination by TRNOE NMR spectroscopy and the saturation transfer difference (STD-NMR) technique of the secondary structure of the peptide P-$Vpu^{41-62}$ bound to the protein $\beta$-TrCP. The residues which are relevant to binding were identified: pSer52, Gly53, Asn54 in the bent region, essentially the pSer phosphate group and the main chain of hydrophobic residues Ile46 and Leu45 in the 44−48 cytoplasmic domain of P-$Vpu^{41-62}$. These results suggest that the WD phosphorecognition domain of $\beta$-TrCP exhibits a dominant positive electrostatic potential, certainly generated by Arg or Lys residues. These residues make direct contact with the phosphate group, thus being essential for function. The main chain position of Ile46 and Leu45 probably lies in close proximity to a second hydrophobic pocket. As shown here, STD-NMR spectroscopy is really well adapted for a fast and reliable method for analyzing $\beta$-TrCP binding processes, as it is for screening various peptides and mapping of ligand epitopes.

## SUPPORTING INFORMATION AVAILABLE

Tables listing $^{13}C$ NMR chemical shifts of the free P-Vpu$^{41-62}$ and of the peptide bound to the protein $\beta$-TrCP from HSQC spectra and dihedral angles of the peptide P-Vpu$^{41-62}$ bound to the protein $\beta$-TrCP assessed by MD calculations with ARIA; figures showing SDS−PAGE analysis of GST-$\beta$-TrCP after purification and binding to glutathione−Sepharose, Western blot analysis of the eluted GST-$\beta$-TrCP protein using anti-$\beta$-TrCP polyclonal antibodies, TRNOESY spectrum of the P-Vpu$^{41-62}$ peptide and a NOESY spectrum of a control sample of Vpu$^{41-62}$ peptide (nonphosphorylated) in the presence of the GST-$\beta$-TrCP protein, 1D $^1H$ and 1D $^1H$ STD-NMR spectra of P-Vpu$^{41-62}$ in complex with the GST-$\beta$-TrCP protein showing glutathione signals present in the 1D $^1H$ and absent in the 1D $^1H$ STD-NMR spectra, and 1D $^1H$ and 1D $^1H$ STD-NMR spectra of control samples with Vpu$^{41-62}$ peptide (nonphosphorylated) and GST-$\beta$-TrCP protein. This material is available free of charge via the Internet at http://pubs.acs.org.

## REFERENCES


1. Strebel, K., Klimkait, T., and Martin, M. A. (1988) *Science 241*, 1221−1223.
2. Cohen, E. A., Terwilliger, E. F., Sodroski, J. G., and Haseltine, W. A. (1988) *Nature 334*, 532−534.
3. Marassi, F. M., Ma, C., Gratkowski, H., Straus, S. K., Strebel, K., Oblatt-Montal, M., Montal, M., and Opella, S. J. (1999) *Proc. Natl. Acad. Sci. U.S.A. 96*, 14336−14341.
4. Strebel, K., Klimkait, T., Maldarelli, F., and Martin, M. A. (1989) *J. Virol. 63*, 3784−3791.
5. Willey, R. L., Maldarelli, F., Martin, M. A., and Strebel, K. (1992) *J. Virol. 66*, 7193−7200.
6. Margottin, F., Bour, S., Durand, H., Selig, L., Benichou, S., Richard, V., Thomas, D., Strebel, K., and Benarous, R. (1998) *Mol. Cell 1*, 565−574.
7. Bour, S., Perrin, C., and Strebel, K. (1999) *J. Biol. Chem. 274*, 33800−33806.
8. Bour, S., Schubert, U., and Strebel, K. (1995) *J. Virol. 69*, 1510−1520.
9. Schubert, U., Bour, S., Ferrer-Montiel, A. V., Montal, M., Maldarelli, M., and Strebel, K. (1996) *J. Virol. 70*, 809−819.
10. Paul, M., and Jabbar, M. A. (1997) *Virology 232*, 207−216.
11. Tiganos, E., Yao, X. J., Friborg, J., Daniel, N., and Cohen, E. A. (1997) *J. Virol. 71*, 4452−4460.
12. Vincent, M. J., and Jabbar, M. A. (1995) *Virology 214*, 639−649.
13. Schubert, U., and Strebel, K. (1994) *J. Virol. 68*, 2260−2271.
14. Schubert, U., Anton, L. C., Bacik, I., Cox, J. H., Bour, S., Bennink, J. R., Orlowski, M., Strebel, K., and Yewdell, J. W. (1998) *J. Virol. 72*, 2280−2288.
15. Fujita, K., Omura, S., and Silver, J. (1997) *J. Gen. Virol. 78*, 619−625.
16. Neer, E. J., Schmidt, C. J., Nambudripad, R., and Smith, T. F. (1994) *Nature 371*, 297−300.
17. Coadou, G., Evrard-Todeschi, N., Gharbi-Benarous, J., Benarous, R., and Girault, J.-P. (2002) *Int. J. Biol. Mol 30*, 23−40.
18. Willbold, D., Hoffmann, S., and Rosch, P. (1997) *Eur. J. Biochem. 245*, 581−588.
19. Ni, F. (1994) *Prog. Nucl. Magn. Reson. Spectrosc. 26*, 517−606.
20. Verdier, L., Gharbi-Benarous, J., Bertho, G., Mauvais, P., and Girault, J. P. (2002) *Biochemistry 41*, 4218−4229.
21. Mayer, M., and Meyer, B. (1999) *Angew. Chem., Int. Ed. Engl. 38*, 1784−1788.
22. Klein, J., Meinecke, R., Mayer, M., and Meyer, B. (1999) *J. Am. Chem. Soc. 121*, 5336−5337.
23. Mayer, M., and Meyer, B. (2001) *J. Am. Chem. Soc. 123*, 6108−6117.
24. Piotto, M., Saudek, V., and Sklenar, V. (1992) *J. Biol. NMR 2*, 661−665.
25. Schleucher, J., Schwendinger, M., Sattler, M., Schmidt, P., Schedletzky, O., Glaser, S. J., Sorensen, O. W., and Griesinger, C. (1994) *J. Biomol. NMR 4*, 301−306.
26. Wüthrich, K. (1986) *NMR of Proteins and Nucleic Acids*, John Wiley & Sons, New York.
27. Nilges, M., and O'Donoghue, S. (1998) *Prog. NMR Spectrosc. 32*, 107−139.
28. Linge, J., and Nilges, M. (1999) *J. Biomol. NMR 13*, 51−59.
29. Brünger, A. T., Adams, P. D., Clore, G. M., DeLano, W. L., Gros, P., Grosse-Kunstleve, R. W., Jiang, J. S., Kuszewski, J., Nilges, M., Pannu, N. S., Read, R. J., Rice, L. M., Smonson, T., and Warren, G. L. (1998) *Acta Crystallogr. D54*, 905−921.
30. Brooks, B. R., Bruccoleri, R. E., Olafson, B. D., States, D. J., Swaminathan, S., and Karplus, M. (1983) *J. Comput. Chem. 4*, 187−217.
31. Schibli, D. J., Monelero, R. C., and Vogel, H. J. (2001) *Biochemistry 40*, 9570−9578.
32. Vranken, W., Tolkatchev, D., Xu, P., Tanha, J., Chen, Z., Narang, S., and Ni, F. (2002) *Biochemistry 41*, 8750−8579.
33. Laskowski, R. A., Rullmann, J. A. C., MacArthur, M. W., Kaptein, R., and Thornton, J. M. (1996) *J. Biomol. NMR 8*, 477−486.
34. Koradi, R., Billeter, M., and Wüthrich, K. (1996) *J. Mol. Graphics 14*, 51−55.
35. Verdier, L., Gharbi-Benarous, J., Bertho, G., Evrard-Todeschi, N., Mauvais, P., and Girault, J.-P. (2000) *J. Chem. Soc., Perkin Trans. 2*, 2363−2371.
36. Margottin, F., Benichou, S., Durand, H., Richard, V., Liu, L. X., Gomas, E., and Benarous, R. (1996) *Virology 223*, 381−386.
37. Chen, M. Y., Maldarelli, F., Karczewski, M. K., Willey, R. L., and Strebel, K. (1993) *J. Virol. 67*, 3877−3884.
38. Zheng, S., Strzalka, J., Ma, C., Opella, S. J., Ocko, B. M., and Blasie, J. K. (2001) *Biophys. J. 80*, 1837−1850.
39. Federau, T., Schubert, U., Flossdorf, J., Henklein, P., Schomburg, D., and Wray, V. (1996) *Int. J. Pept. Protein Res. 47*, 297−310.
40. Lassot, I., Ségéral, E., Berlioz-Torrent, C., Durand, H., Groussin, L., Hai, T., Benarous, R., and Margottin-Goguet, F. (2001) *Mol. Cell. Biol. 21*, 1−11.
41. Williams, R. E. (1976) *Science 192*, 473−474.
42. Hol, W. G. J., van Duijnen, P. T., and Berendsen, H. J. C. (1978) *Nature 273*, 443−446.
43. Bai, C., Sen, P., Hofmann, K., Ma, L., Goebl, M., Harper, J., and Elledge, S. (1996) *Cell 86*, 263−274.
44. Orlicky, S., Tang, X., Willems, A., Tyers, M., and Sicheri, F. (2003) *Cell 112*, 243−256.
45. ter Haar, E., Harrison, S. C., and Kirchhausen, T. (2000) *Proc. Natl. Acad. Sci. U.S.A. 97*, 1096−1100.
46. Steele, M. R., McCahill, A., Thompson, D. S., MacKenzie, C., Isaacs, N. W., Houslay, M. D., and Bolger, G. B. (2001) *Cell. Signalling 13*, 507−513.
47. Davis, M., Hatzubai, A., Andersen, J. S., Ben-Shushan, E., Zvi Fisher, G., Yaron, A., Bauskin, A., Mercurio, F., Mann, M., and Ben-Neriah, Y. (2002) *Genes Dev. 16*, 439−451.
48. Nash, P., Tang, X., Orlicky, S., Chen, Q., Gertler, F. B., Mendenhall, M. D., Sicheri, F., Pawson, T., and Tyers, M. (2001) *Nature 414*, 514−521.
49. Spruck, C. H., Strohmaier, H., Sangfelt, O., Muller, H. M., Hubaleck, M., Muller-Hozner, E., Marth, C., Widschwendter, M., and Reed, S. I. (2002) *Cancer Res. 62*, 4535−4539.
50. Strohmaier, H., Spruck, C. H., Kaiser, P., Won, K. A., Sangfelt, O., and Reed, S. I. (2001) *Nature 413*, 316−322.
51. Yaffe, M. B., and Elia, A. E. (2001) *Curr. Opin. Cell Biol. 13*, 131−138.


BI035207U